CO AND DUST PRODUCTIONS IN 67P/CHURYUMOV-GERASIMENKO AT 3 AU POST-PERIHELION

D. Bockelée-Morvan, R. Moreno, N. Biver, J. Crovisier
LESIA, Observatoire de Paris, 5 place Jules Janssen, F-92195, France
dominique.bockelee@obspm.fr

J.-F. Crifo
Service d'Aéronomie, BP3, F-91371, Verrières Le Buisson Cedex, France

M. Fulle
Osservatorio Astronomico di Trieste, Via Tiepolo 11, I-4131, Trieste, Italy

M. Grewing
Institut de radioastronomie millimétrique, 300 rue de la Piscine, Domaine universitaire, F-38406, St-Martin-d'Hères, France

Abstract Following the selection of comet 67P/Churyumov-Gerasimenko as the new target of the *Rosetta/ESA* mission, observations of this comet were performed at the 30-m telescope of the Institut de radioastronomie millimétrique in May–June 2003. Observations focussed on the CO J(2–1) and J(1–0) lines and dust thermal continuum at 1.2 mm in order to constrain the CO and dust productions at 3 AU from the Sun. Neither the CO lines, nor the continuum emission were detected. The derived 3–σ upper limit on the CO production rate is $Q_{\rm CO} < 9.2 \times 10^{26}$ molecules s^{-1}. That derived for the dust production rate is strongly model dependent, and at best $Q_{\rm dust} < 36$ kg s^{-1}. The first synthetic CO line profiles computed with a 3-D gas-dynamical simulation of a gas coma are presented.

Keywords: 67P/Churyumov-Gerasimenko, CO, dust, radio observations, Rosetta

Introduction

In spring 2003, the European Space Agency selected comet 67P/Churyumov-Gerasimenko (hereafter designated as 67P) as the new target of the *Rosetta* mission. Strong effort was requested to obtain information on this comet. From analysis of wide field images, where the neck line is visible, it was inferred that 67P released large quantity of 1 cm-sized particles in 2002 at 2 AU pre-perihelion (Fulle et al. 2004a, b). This finding, which implies high gas production, motivated CO and continuum observations at millimetre wavelengths in May–June 2003, when the comet was at 3 AU from the Sun, post-perihelion. Millimetre observations are more sensitive than IR or UV observations to detect CO at large heliocentric distances. Continuum flux radiation in the millimetre spectral range is dominated by thermal radiation of mm-sized particles, which contain a large fraction of the total grain mass. We present here observations which were undertaken with the 30-m telescope of the Institut de radioastronomie millimétrique (IRAM) on Pico Veleta (Spain).

1. CO and HCN

Observations

The observations of the CO lines were carried out on 2 and 3 May UT and from 20 to 24 May UT, 2003, when the comet was at $r_h \sim 3$ AU from the Sun post-perihelion, and at Δ = 2.27–2.70 AU from the Earth. A log of the observations is given in Table 1. Four receivers were used at the same time. The A100 and B100 receivers were tuned to the frequency of the CO $J(1\text{–}0)$ line (115.271 GHz). The A230 and B230 receivers were tuned to that of CO $J(2\text{–}1)$ (230.538 GHz). On 24 May, part of the observations were made with the B100 receiver tuned to the HCN $J(1\text{–}0)$ line at 88.632 GHz. The receivers were connected to the autocorrelator *VESPA* divided in four units of 35 MHz bandwidth and 19.5 kHz spectral resolution, corresponding to a velocity resolution of 0.051 and 0.025 km s^{-1} for the $J(1\text{–}0)$ and $J(2\text{–}1)$ lines, respectively. The receivers were also connected to low resolution (0.3 to 1.25 MHz) backends for redundancy and checking purposes. In order to increase the sensitivity of the measurements, the observations were performed using the frequency switching mode with a frequency throw of 6.5 MHz for the A230/B230 receivers, and of 7 MHz for the A100/B100 receivers. The weather conditions were generally good, with typical SSB system temperatures at comet transit ($\sim$65° elevation) in the range 220–240 K (115 GHz) and 320–400 K (230 GHz) in the T_A^* scale.

On each day, the comet observations were preceded by line observations of IRC+10216 using the same instrumental set-up, in order to check that the receivers and spectrometers were operating well. The detection of the strong

Table 1. Log of the observations of comet 67P at the IRAM 30-m telescope

Date (UT)	r_h (AU)	Δ (AU)	Obs.	Integ.[a] (min)	Offset[b] (")	r.m.s.[c]
2003 May 2	2.87	2.27	CO $J(1–0)$	190	2.0	17 mK
			CO $J(2–1)$	190	2.0	25 mK
2003 May 3	2.88	2.29	CO $J(1–0)$	170	2.0	18 mK
			CO $J(2–1)$	170	2.0	29 mK
2003 May 20	2.99	2.62	CO $J(1–0)$	400	3.4	14 mK
			CO $J(2–1)$	390	3.4	29 mK
2003 May 21	3.00	2.64	CO $J(1–0)$	580	3.1	12 mK
			CO $J(2–1)$	580	3.1	17 mK
2003 May 22	3.00	2.66	CO $J(1–0)$	460	5.0	10 mK
			CO $J(2–1)$	440	5.0	13 mK
2003 May 23	3.01	2.68	CO $J(1–0)$	500	3.8	11 mK
			CO $J(2–1)$	490	3.8	13 mK
2003 May 24	3.02	2.70	CO $J(1–0)$	90	1.9	27 mK
			CO $J(2–1)$	180	1.9	21 mK
			HCN $J(1–0)$	90	1.9	10 mK
2003 June 13	3.15	3.10	cont. 250 GHz	90	0.0	1.3 mJy
2003 June 16	3.17	3.17	cont. 250 GHz	60	0.0	1.2 mJy

[a] total integration time on source;
[b] pointing error for the B100/B230 receivers;
[c] for lines, r.m.s. in T_A^* for a 19.5 kHz resolution channel.

mesospheric CO lines in the frequency-switch spectra of comet 67P provided an additional check that the system was working well.

The comet was tracked using osculating orbital elements taken from the JPL's Horizons System (http://ssd.jpl.nasa.gov/horizons.html). To check and correct the absolute pointing of the telescope, continuum sources close to the comet were regularly observed with the B100 receiver tuned at 115 GHz. Because of the faintness of the continuum pointing sources and of atmospheric instabilities, adopted pointing corrections were not always optimum during the 20–24 May period. Pointing errors were evaluated afterwards, and range from 2 to 5" depending of the date, as given in Table 1. The mean offsets for the average 2–3 May and 20–24 May CO observations are 2.6 and 4.3", respectively (Table 2). These offsets include the misalignment (2.4" in azimuth) of the A100/A230 receivers with respect to the B100/B230 receivers.

The half-power beam width (*HPBW*) was evaluated to 21" at 115 GHz and to 10.7" at 230 GHz, from continuum observations of Jupiter performed during the observing run. The main beam efficiencies measured on this planet are 0.75 and 0.55, at 115 and 230 GHz, respectively.

The total integration time on the comet was $\sim$2400 min on each CO line, adding the time spent on each receiver. The CO $J(1–0)$ and $J(2–1)$ lines were not detected. Table 2 summarizes the results of the observations.

Table 2. Summary of CO and HCN observations

Date	r_h (AU)	Δ (AU)	Offset[a] (")	line	Integ.[b] (min)	$\int T_{mB} dv^c$ (mK km s^{-1})	Q (10^{27} s^{-1})
May 2–3	2.87	2.28	2.6	CO J(1–0)	360	< 14	< 6.0
				CO J(2–1)	360	< 19	< 2.1
May 20–24	3.00	2.66	4.3	CO J(1–0)	2200	< 5.8	< 3.1
				CO J(2–1)	2080	< 7.2	< 1.0
May 24	3.02	2.70	2.0	HCN J(1–0)	90	< 22	< 0.016

[a] includes 2.4" misalignment between 230 and B230 receivers;
[b] total integration time on source;
[c] 3–σ upper limit over –1.0 to 0.6 km s^{-1} velocity interval.

Modelling and results on CO production

Models have been developed in order to interpret intensities of molecular millimetric lines in terms of gas production rate (e.g., Crovisier 1987; Biver et al. 1999a). These models follow a two-step process. First, the evolution of the population of the rotational levels within the ground vibrational state is computed as the molecules expand in the coma along a radial direction. The excitation model takes into account the main excitation processes, which are collisions, excitation of the infrared bands by the Sun radiation and, for comets at heliocentric distances larger than 3 AU, excitation by the 3 K cosmic background (Biver 1997). For CO under optically thin conditions, which applies here, the input parameters are the gas temperature T and the expansion velocity v_{exp} throughout the coma, the neutral–neutral cross-sections σ_c and the density distribution of the collision partners. These two last parameters control the size of the inner coma region where the populations are at local thermal equilibrium before evolving towards fluorescence equilibrium. Collisions between CO and electrons have no significant impact on CO excitation, because the dipole moment of CO is small (Biver et al. 1999a). In the second step, the radiative transfer equation is solved and provides the line intensity within the antenna beam, to be compared to the observations. A synthetic line profile can also be computed, taking into account thermal broadening. In the current state of the model, a Maxwellian thermal velocity distribution defined by the temperature is used, though this does not apply when the flow becomes free-molecular.

In most interpretations, the molecular density of the considered species (here CO) and collision partner (H_2O and/or CO) is described by a Haser law, the gas temperature and velocity are assumed to be constant throughout the coma, and the coma is isotropic. The input pararameters are constrained by observations (e.g., v_{exp} from the line profile) or guessed (see, e.g., Biver et al. 1999a). A gas production rate is then derived.

Table 3. Model parameters

Gas model	Q_{CO} (s^{-1})	Q_{CO} day/night	Q_{H_2O} (s^{-1})	Nucleus
1	10^{27}	$\sim 1^a$	0	2-km sphere
2	10^{27}	19^b	0	2-km sphere
3	5.45×10^{26}	$\sim 1^a$	4×10^{26}	2-km sphere
4	5.09×10^{26}	19^b	4×10^{26}	2-km sphere
5	10^{27}	1^a	2.5×10^{26}	"starfish"

[a] corresponds to asymmetry parameter a_0 = 0.9 defined in Crifo et al. (2004);
[b] corresponds to asymmetry parameter a_0 = 0.1.

A more advanced approach was used here, taking advantage of gas dynamical 3-D models described in Crifo et al. (2004). This approach was motivated by: i) the absence of observational constraints on the physical parameters of a rarefied coma as that of 67P at 3 AU from the Sun; ii) the need to prepare the exploitation of the spectral data that will be acquired by the *MIRO* microwave experiment on *Rosetta*; iii) last but not least, the concern to provide an accurate constraint on CO production in 67P at 3 AU from the Sun.

Gas dynamical 3-D calculations were performed for 67P at 3 AU from the Sun for various CO/H_2O gas production models and nucleus shapes (Crifo et al. 2004). Five models are considered here, which parameters are given in Table 3. CO production from the surface is either almost uniform (models 1, 3 and 5) or strongly asymmetric (models 2 and 4). For the mixed CO/H_2O models (models 3–5), H_2O ice is distributed uniformly on the surface, but sublimates according to the solar illumination. For models 1–4, the nucleus is a 2 km radius sphere. In model 5, the nucleus has a "starfish" analytical shape (it mimics the shape proposed by Lamy et al. (2003) for the nucleus of 67P). Models 1 and 5 are presented in details in Crifo et al. (2004).

The gas dynamical calculations provide the distributions of T, v_{exp}, CO and H_2O (for CO-H_2O mixtures) densities (n_{CO}, n_{H_2O}) distributions in the coma out to a distance $D \sim 10^5$ km. However, above some much closer distance in the coma, the flow becomes practically free-molecular, and the gas velocity distribution ceases to be Maxwellian. One can then define a "parallel temperature" $T_{||}$ and a "perpendicular temperature" $T_{\perp}$ which differ. $T_{||}$ and the velocity vector freeze-out, while $T_{\perp}$ decreases to zero. These freezing-out are not present in the gas dynamical solutions. Direct Simulation Monte Carlo (DSMC) calculations performed up to 40 km from the nucleus for model 1 show excellent agreement with the fluid approach for T and v_{exp} in this region (Crifo et al. 2004), but reveal that the freezing-out of $T_{||}$ proceeds above 2–4 km above the surface. Thus, for this model, we present results assuming frozen T and velocity vector beyond D = 40 km. For models 1 and 2, we also present calculations with the full gas dynamical results (D = 80 000 km).

Table 4. Model results for the CO J(2–1) line

Gas model	D^a (km)	$v_{exp}{}^b$ (km s^{-1})		T^b (K)		$\int T_{mB} dv^c$ (mK km s^{-1})	$n_u{}^d$	N^e 10^{31}
		Sun	anti-Sun	Sun	anti-Sun			
1	40	0.74	0.38	15	4	9.2	0.22	3.28
	80 000	0.77	0.45	40	71	9.0	0.22	3.13
2	40	0.74	0.38	14	4	9.1	0.26	2.77
	80 000	0.77	0.45	40	74	7.7	0.22	2.68
3	40	0.77	0.51	14	7	4.3	0.25	1.34
4	40	0.76	0.51	14	7	4.7	0.26	1.38
5	40	0.76	0.52	12	6	7.5	0.23	2.53

[a] distance above which the velocity vector and T are frozen;
[b] terminal velocity and temperature;
[c] line area of the CO J(2–1) line for the IRAM observing conditions on May 20–24, 2003, but with a beam offset equal to 0. For models 1–4, the Earth-comet-Sun angle (i.e., phase angle) is taken equal to 0°; results with phase angle = 19° (corresponding to 67P in May 2003) are similar within 1%. For model 5, the line of sight is along the smallest nucleus axis, and the phase angle is 45°;
[d] mean population of the J = 2 CO rotational level probed by the IRAM beam;
[e] number of molecules probed by the IRAM beam; see other parameters in footnote c).

Table 4 gives the terminal temperature and expansion velocity in the Sun and anti-Sun directions for the physical models considered here.

The resulting 3-D distributions of T, v_{exp}, n are used to compute the 3-D distribution of the populations of the CO rotational levels, and then synthetic line profiles. The time-dependent excitation model is run along radial rays, which assumes implicitly that the molecules flow outwards radially (and this is indeed almost the case). The total CO–CO cross-section for collisional de-excitation is taken equal to 2×10^{-14} cm^2. That for CO–H_2O is 5×10^{-14} cm^2. These cross-sections are poorly known.

The computed CO J(2–1) line intensities for the observing conditions at IRAM on 20–24 May 2003 are given in Table 4. When scaled to the same CO production rate, all models give consistent results within 20%, with most of them within 8%. There are two reasons for that. First, the molecules probed by the IRAM beam ($\sim$ 10 300 radius) have about the same excitation state for all models (see the mean population n_u of the J = 2 state in Table 4). These molecules have not reached yet fluorescence equilibrium (where n_u = 0.15) but are at altitudes where collisional excitation is not significant. Second, the number of molecules N probed by the IRAM beam does not vary much with the model (see Table 4). The derived 3–σ $Q_{\rm CO}$ upper limit, taking into account the beam offset, is 10^{27} s^{-1} for the 20–24 May period (Table 2), and 9.2×10^{26} s^{-1} when including the 2–3 May observations. The upper limit derived from the J(1–0) line is three times higher (Table 2).

Synthetic line profiles are shown in Fig. 1. The two spectra in Fig. 1A (model 1, with D = 40 km and D = 80 000 km) illustrate the effect of terminal velocity and temperature on the line shape. The spectra for model 1 (Fig. 1A) present a strong peak towards positive velocities, because the coma is more dense on the night side. In contrast, for model 2, the CO coma is more dense in the day side: on the corresponding spectrum (Fig. 1B), the strong peak is at a negative velocity. The features seen at 0.15–0.20 km s^{-1} on these spectra are real and trace the relatively dense conical structure (weak shock) formed in the night side coma, near the terminator, to match the supersonic flows originating from the dayside nucleus surface to that originating from the night-side nucleus surface.

Fig. 1C shows the synthetic line profile for the "starfish" nucleus, with the line of sight along the smallest nucleus axis (see Fig 1 of Crifo et al. 2004; the phase angle is 45°). In this case, the coma is structured by the nucleus topography. These synthetic profiles prefigure the spectra which will be obtained by the *MIRO* experiment onboard *Rosetta*.

Upper limit on HCN production

The observations of HCN made on 24 May 2003 were analysed with the excitation model presented in Biver (1999a), in the simple case of an isotropic HCN coma with v_{exp} = 0.6 km s^{-1} and T = 15 K. The derived upper limit on the HCN production rate is $Q_{\rm HCN}$ < 1.6 $\times$ 10^{25} s^{-1}, and is ten times larger that the CN production rate determined by Schulz et al. (2004) for beginning of May, from observations at the European Southern Observatory.

2. Dust

Observations

The continuum observations of comet 67P were performed on 13 and 16 June 2003. We used the Max Planck Institut für Radioastronomie bolometer array with 117 pixels (*MAMBO-2*). Pixels are separated by $\sim$ 20", and their half-power beam width is 11". The effective frequency is close to 250 GHz, and the total bandwidth is about 60 GHz. Observations of comet 67P were performed using the ON–OFF mode, where the subreflector of the telescope is alternatively looking at the target and at a position 32" away in azimuth with a rate of 2 Hz. This observing technique subtracts most of the atmospheric emission. Some weak atmospheric continuum residuals remain, due to fast temporal fluctuations of the terrestrial atmosphere. The multi-beam observations allow us to measure these residuals from the channels adjacent to the central channel.

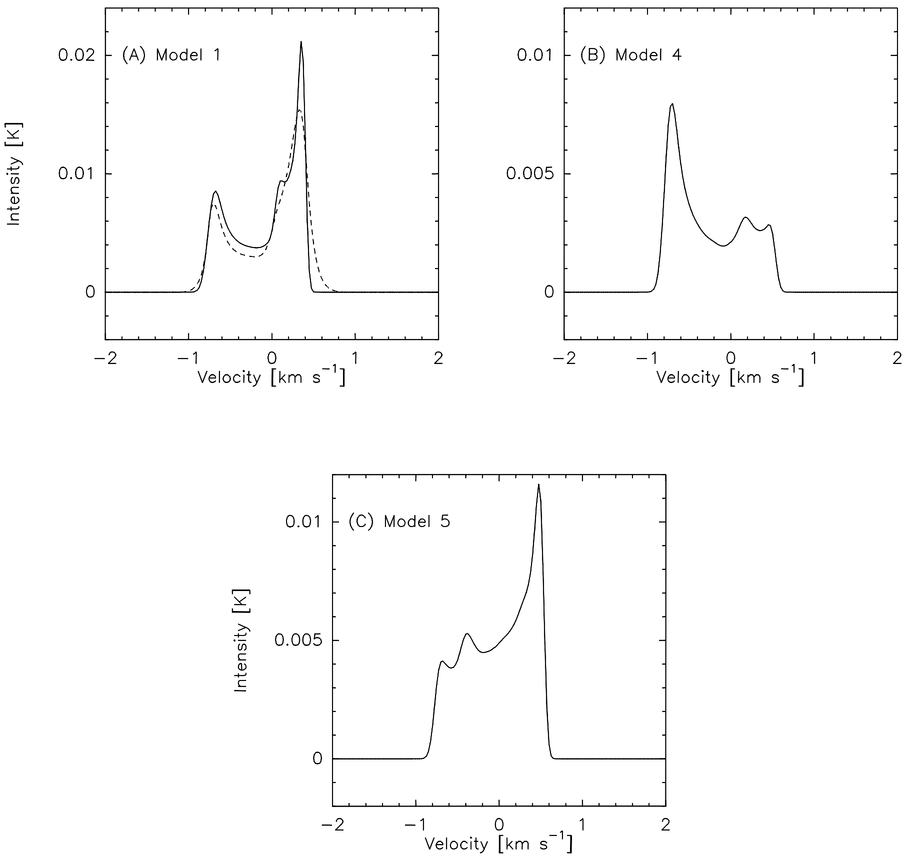

Figure 1. Synthetic CO J(2–1) line profiles for the IRAM observing conditions of 20–24 May 2003. (A) Model 1 (uniform CO production) with D = 40 km (plain line) and D = 80000 km (dashed line); (B) Model 4 (asymmetric CO production) with D = 40 km. (C) Model 5 (starfish nucleus shape with uniform CO production) with D = 40 km. For (A) and (B), the phase angle is taken equal to 0°. For (C), the line of sight is along the smallest nucleus axis and the phase angle is 45°. The spectral resolution is 0.025 km s^{-1}.

All bolometric measurements were obtained by observing remotely from Grenoble (France). Flux calibration was determined through observations of Jupiter, Uranus, and Mars. The pointing and focus of the telescope were achieved by observing the quasar 3C273. Sky observations at several elevations (skydip) permitted us to measure the zenithal atmospheric opacity. Observations were performed in average weather conditions (zenithal sky opacity = 0.25–0.50), but with good atmospheric stability. ON–OFF observations were taken during $\sim$ 1 hour per day, and the results are summarized in Table 1.

The data reduction was performed using the NIC softwares. The basic reduction process consists in: i) removing data spikes; ii) computing the ON minus OFF phases; iii) eliminating the sky noise by applying a noise removal algorithm based on beam to beam correlation; iv) correcting the central channel flux from the mean flux observed on adjacent channels, in order to remove possible residual continuum offsets.

We finally conclude that the comet dust continuum is not detected in our bolometric observations and will adopt a 1–σ upper limit of 1 mJy for its 1.2 mm flux.

Upper limit on dust production

Continuum flux radiation in the millimetre spectral range is dominated by thermal emission from cometary solids, mainly dust when the comet is active. (an order of magnitude for the thermal emission from the nucleus of 67P is 0.02 mJy at 1.2 mm, obtained by assuming a 2 km radius sphere and a surface temperature T = 182 K). To interpret the observations in terms of dust production, we followed the simple approach described by Jewitt and Luu (1992). As a first approximation, the temperature of the grains is taken to be the blackbody equilibrium temperature for a fast rotator (154 K at 3.15 AU). Indeed, though submicrometric grains may be superheated with respect to the blackbody temperature, they are inefficient emitters of millimetre radiation. From this, we deduce a 1–σ upper limit for the effective blackbody cross-section at 1.2 mm of 7.5 $\times$ 10^8 m^2 within the IRAM beam.

The blackbody cross-section $C(\lambda)$ is related to the grain mass M by $C(\lambda) = \kappa(\lambda)M$, where $\kappa(\lambda)$ (m^2 kg^{-1}) is the opacity at wavelength λ. κ is a function of particle size distribution, composition, shape, and varies with λ. There is a large uncertainty on the value of κ(1 mm) pertaining to cometary dust. Values adopted in the literature range from 0.05 m^2 kg^{-1} (Jewitt and Matthews 1997) to 7.5 m^2 kg^{-1} (Altenhoff et al. 1999). The former value is that modelled for interstellar (submicrometric) dust, while the latter value characterizes the β Pictoris circumstellar dust dominated by mm-sized particles (see the discussion in Altenhoff et al. 1999). Using this range of κ(1 mm), we infer an upper limit on M in the range 8.4 $\times$ 10^7 kg to 1.3 $\times$ 10^{10} kg, the smaller value corresponding to the β Pictoris κ value.

In Jewitt and Luu (1992) and following papers, the dust mass production rate Q_d is related to M by the approximate formula Q_d = M/t, where $t = p/v_d$ is the residence time of the dust particles in the projected beam of radius p, and v_d is the velocity of the grains emitting efficiently at the observed frequency. For grains that are expanding radially and isotropically, the exact formula (which we use here) is Q_d = $2\alpha v_d M/\pi p$, where α = 0.94 is a coefficient which accounts for the Gaussian shape of the beam (α = 1 for a circular aperture) and p = *HPBW*/2.

Multi-wavelength observations in the millimetre-submillimetre range showed that the particles dominating the thermal continuum at 1 mm are typically 1-mm sized. The velocity of such particles in the coma of 67P is uncertain. The calculations performed by Crifo et al. (2004) with the gas production model 1 (see Section 1) give a maximal terminal velocity of 1 m s $^{-1}$ for spherical grains with a = 9 mm radius and specific density ρ_d = 0.1 g cm^{-3}. As $v_d \propto a^{-0.5}$, v_d(1 mm) $\sim$ 3 m s^{-1}. For grains with ρ_d = 1 g cm^{-3}, v_d(1 mm) is expected $\sim$ 1 m s^{-1}. Conservatively, we assumed v_d(1 mm) = 3 m s^{-1}. The inferred (1–σ) upper limit on dust production Q_d is 12.2 kg s^{-1} for κ(1 mm) = 7.5 m^2 kg^{-1}, and 1.9$\times$10^3 kg s^{-1} for κ(1 mm) = 0.05 m^2 kg^{-1}. Better constraints (likely intermediate between these two values) could be obtained using detailed modelling of dust temperature, emissivity, dynamics, and size distribution, but this is beyond the scope of this paper.

3. Discussion

Let us compare the preceding upper limits to other available informations about the gas and dust production, post-perihelion. There exist observations relative to a post-perihelion heliocentric distance $\simeq$ 2.5 AU (March 2003). From photometric measurements in the visible performed during this period, Kidger (2003) inferred Q_d =1–2 kg s^{-1}. On the other hand, from studies of the dust tail, Fulle et al. (2004a, b) estimated Q_d to $\sim$ 5–10 kg s^{-1}. The discrepancy between these estimates is not surprising, as visible light photometry is usually insensitive to large dust grains, where most of the ejected mass often lies. Anyhow, these two estimates are well below our present upper limit (at best $<$ 36 kg s^{-1} at 3–σ). Fulle et al. (2004a, b) also determined the dust size distribution, which was found steep, with a maximum size $\sim$ 4 mm. From the well-known balance condition between aerodynamic drag and gravity at the surface, we compute that to eject mm-sized spherical grains from a 2 km radius comet requires a gas production rate (CO and other species) of about 10^{27} s^{-1}, if the nucleus and dust grains specific masses are both equal to 1 g cm^{-3}. Even smaller rates would eject such grains if their specific mass was smaller and/or if their shape was markedly aspherical. Our present $Q_{\rm CO}$ upper limit suggests that this is the case, or that the total (CO+H_2O) production rate reached 10^{27} s^{-1} at 2.5 AU.

Which other constraints can be put on the CO production rate of 67P at 3 AU from the Sun? The water production rate at perihelion (q = 1.3 AU) is $\sim 10^{28}$ s^{-1} (see several papers in this book). There are only few constraints on the CO production rate relative to water in Jupiter-family comets near 1 AU from the Sun (see, e.g., Bockelée-Morvan et al. 2004), but reasonnable values are between 1–10%, or even lower. Then, if the CO production is almost constant along the orbit, as predicted by thermal evolution models of cometary nuclei, $Q_{\rm CO}$ is expected to be, at 3 AU, in the range 10^{26} – 10^{27} s^{-1}. If, on the contrary, it follows the r_h^{-2} heliocentric dependence observed in comet Hale-Bopp for $Q_{\rm CO}$ (Biver et al. 1999b), we expect $Q_{\rm CO}$ in the range 2×10^{25} – 2×10^{26} s^{-1}. Finally, another estimate can be obtained from the total visual magnitude-to-$Q_{\rm CO}$ empirical correlation established by Biver (2001) from observations of comet Hale-Bopp and other comets, which leads here to $Q_{\rm CO} \sim 10^{26}$ s^{-1} at 3 AU post-perihelion.

To summarize, these indirect estimates suggest a low CO production rate at 3 AU on the order 10^{26} s^{-1}, with an uncertainty of an order of magnitude by excess of by default. This uncertainty leaves us with practically the full range of scenarii for the future *Rosetta* landing, e.g. negligible to dominant aerodynamic perturbations on the orbiter. But, in addition, what we are much more interested in knowing, is the production rate of the comet at 3 AU *pre-perihelion* – because the *Rosetta* encounter is scheduled there. There are indications that the comet is much more active pre- than post-perihelion (Fulle et al. 2004a, b). For these reasons, it will be useful to attempt pre-perihelion observations of CO and dust thermal emission at its next passage.

References

Altenhoff, W. J. and 20 colleagues (1999). Coordinated radio continuum observations of comets Hyakutake and Hale-Bopp from 22 to 860 GHz. *Astron. Astrophys.*, 348:1020–1034.

Biver, N. (1997). Molécules mères cométaires: observations et modélisations. PhD thesis, University of Paris 7.

Biver, N. (2001). Correlation between visual magnitudes and the outgassing rate of CO in comets beyond 3 AU. *International Comet Quarterly*, 23:85–93.

Biver N. and 13 colleagues (1999a). Spectroscopic monitoring of comet C/1996 B2 (Hyakutake) with the JCMT and IRAM radio telescopes. *Astron. J.*, 118:1850–1872.

Biver, N. and 22 colleagues (1999b). Long-term evolution of the outgassing of comet Hale-Bopp from radio observations. *Earth Moon and Planets*, 78:5–11.

Bockelée-Morvan, D., Biver, N., Colom, P., Crovisier, J., Henry, F. Lecacheux, A., Davies, J. K., Dent, W. R. F., and Weaver, H. A. (2004). The outgassing and composition of Comet 19P/Borrelly from radio observations. *Icarus*, 167:113–128.

Crifo, J.F., Lukyanov, G.A., Zakharov, V.V., and Rodionov, A.V. (2004). Physical model of the coma of comet 67P/Churyumov-Gerasimenko. This book.

Crovisier J. (1987). Rotational and vibrational synthetic spectra of linear parent molecules in comets. *Astron. Astrophys. Suppl. Ser.*, 68:223–258.

Fulle, M., Barbieri, C., Cremonese, G., Rauer, H., Weiler, M., Milani, A., and Ligustri, R. (2004a). 67P dust environment: a challenge for the Rosetta probe? *Astron. Astrophys.*, submitted for publication.

Fulle, M., Barbieri, C., Cremonese, G., Rauer, H., Weiler, M., Milani, A., and Ligustri, R. (2004b). Dust environment of comet 67P/Churyumov-Gerasimenko. This book.

Jewitt, D., and Luu, J. (1992). Submillimeter continuum emission from comets. *Icarus*, 100:187–196.

Jewitt, D. , and Matthews, H.E. (1997). Submillimeter continuum observations of comet Hyakutake (1996 B2). *Astron. J.*, 113:1145–1151.

Kidger, M. R. (2003). Dust production and coma morphology of 67P/Churyumov-Gerasimenko during the 2002–2003 apparition. *Astron. Astrophys.*, 408: 767–774.

Lamy, Ph., Toth, I., and Weaver, H. (2003). Press release STScI-2003-26.

Schulz, R., Stüve, J.A., and Boehnhardt, H. (2004). Monitoring comet 67P/Churyumov-Gerasimenko from ESO in 2003. This book.